Inorganics **2013**, *1*, 32-45; doi:10.3390/inorganics1010032

OPEN ACCESS

inorganics

ISSN 2304-6740

www.mdpi.com/journal/inorganics

Article

Facile and Selective Synthetic Approach for Ruthenium Complexes Utilizing a Molecular Sieve Effect in the Supporting Ligand

Dai Oyama [1,*], Ayumi Fukuda [1,†], Takashi Yamanaka [1,†] and Tsugiko Takase [2]

[1] Department of Industrial Systems Engineering, Cluster of Science and Engineering, Fukushima University, 1 Kanayagawa, Fukushima 960-1296, Japan; E-Mails: daioyama@yahoo.co.jp (A.F.); s1070050@yahoo.co.jp (T.Y.)

[2] Center for Practical and Project-Based Learning, Cluster of Science and Engineering, Fukushima University, 1 Kanayagawa, Fukushima 960-1296, Japan; E-Mail: ttakase@sss.fukushima-u.ac.jp

† These authors contributed equally to this work.

* Author to whom correspondence should be addressed; E-Mail: daio@sss.fukushima-u.ac.jp; Tel./Fax: +81-24-548-8199.

Received: 21 October 2013; in revised form: 28 November 2013 / Accepted: 3 December 2013 / Published: 9 December 2013

Abstract: It is extremely important for synthetic chemists to control the structure of new compounds. We have constructed ruthenium-based mononuclear complexes with the tridentate 2,6-di(1,8-naphthyridin-2-yl)pyridine (dnp) ligand to investigate a new synthetic approach using a specific coordination space. The synthesis of a family of new ruthenium complexes containing both the dnp and triphenylphosphine (PPh_3) ligands, $[Ru(dnp)(PPh_3)(X)(L)]^{n+}$ (X = PPh_3, NO_2^-, Cl^-, Br^-; L = OH_2, CH_3CN, C_6H_5CN, SCN^-), has been described. All complexes have been spectroscopically characterized in solution, and the nitrile complexes have also been characterized in the solid state through single-crystal X-ray diffraction analysis. Dnp in the present complex system behaves like a "molecular sieve" in ligand replacement reactions. Both experimental data and density functional theory (DFT) calculations suggest that dnp plays a crucial role in the selectivity observed in this study. The results provide useful information toward elucidating this facile and selective synthetic approach to new transition metal complexes.

Keywords: synthesis; ruthenium complex; polypyridyl ligand; crystal structure; DFT calculation

1. Introduction

A more accurate regulation of the structure leads to the construction of appropriate reaction systems. For example, some isomeric pairs of $[Ru(tpy)(L)Cl]^{n+}$ type complexes (tpy = 2,2':6',2''-terpyridine, L = asymmetrical pyridyl-based bidentate ligands; quinaldic acid (qu) and 2-(1-methyl-3-pyrazolyl)pyridine (pypz-Me)) have been prepared and structurally characterized as precatalysts to investigate the effect of isomeric structural features on the catalytic epoxidation process [1,2]. In the complex $[Ru(tpy)(qu)(OH_2)]^+$, the *cis* isomer has been established to be an excellent catalyst for the chemoselective epoxidation through limited differences in electronic structural features exist between the isomeric pair [1]. In the complex $[Ru(tpy)(pypz\text{-}Me)(OH_2)]^{2+}$, on the other hand, the *trans* isomer exhibits better activity because it contains a pyridine C–H bond nearly parallel to the Ru–O bond, whereas for the *cis* isomer this position is occupied by a $C–CH_3$ group and thus exerts a much stronger steric effect [2]. These examples indicate that it is important to clearly distinguish the molecular structures of the compounds. Therefore, much attention has been paid to study both facile and selective synthesis for complex compounds.

In an effort to discover new molecular systems, we have recently reported ruthenium-based mononuclear complexes with the pyridyl-bridged di(1,8-naphthyridin-2-yl) (dnp) ligand [3]. The tridentate dnp has two noncoordinating nitrogen atoms and is able to form intramolecular hydrogen bonds between the coordinated water and dnp. In addition, dnp has a narrower coordination space on the equatorial site than the parent ligand, tpy (Chart 1). Therefore, size complementarity of the entering molecule with the coordination space of dnp plays an important role and is apparent in size-selective recognition of entering molecules such as nitriles and halides. We report that dnp in the present complex system behaves like a "molecular sieve" in ligand replacements and it leads to a facile and selective synthesis of a new family of ruthenium complexes.

Chart 1. Chemical structures of tpy (**left**) and dnp (**right**).

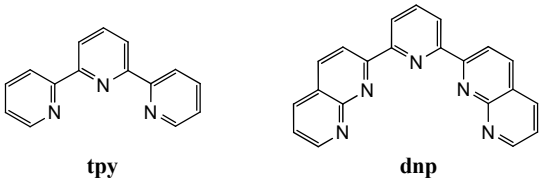

tpy **dnp**

2. Results and Discussion

2.1. Synthesis of Ruthenium Complexes Utilizing the Molecular Sieve Effect of the dnp Ligand

2.1.1. Synthesis of the Precursor

Dnp was prepared by the Friedländer condensation of two equivalents of 2-aminonicotinaldehyde with 2,6-diacetylpyridine according to procedures that have been reported earlier [4,5]. Precursor **1** was synthesized by treating $[RuCl_2(CH_3CN)_2(PPh_3)_2]$ [6] with dnp in an ethanolic solution (Scheme 1). The analogous complexes containing tpy initially formed chlorido complexes, which can only be hydrated with the assistance of the silver ion to cleave the Ru–Cl bond [7,8]. However, the present system spontaneously hydrates under the reaction conditions. Dnp has two additional fused pyridine rings attached to two side-coordinating pyridines of tpy. These rings presumably promote hydration both by electronic repulsion of the chloride leaving group and stabilization of the entering water through hydrogen bonds.

Scheme 1. Preparation of the precursor.

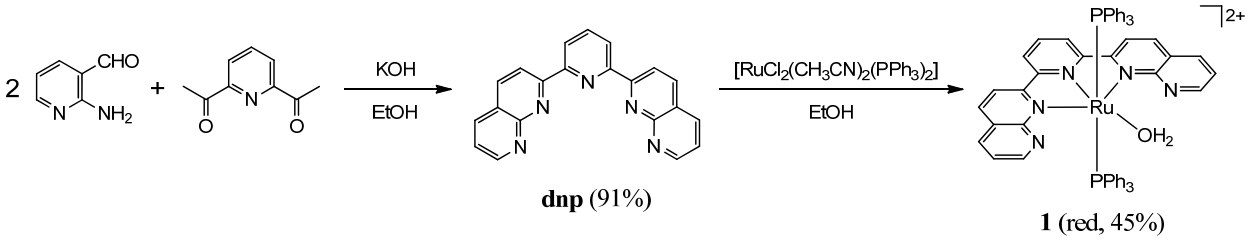

dnp (91%)

1 (red, 45%)

1 was characterized by both ^1H and $^{31}P\{^1H\}$ nuclear magnetic resonance (NMR) spectroscopy in acetone-d_6, and the resulting spectra showed well-resolved signals. A signal observed at 8.23 ppm disappeared on the addition of D_2O, which could be attributed to the protons of the aqua ligand [9]. The $^{31}P\{^1H\}$ NMR spectrum of **1** showed a singlet at 27.29 ppm, which indicates two triphenylphosphine (PPh_3) ligands situated *trans* to each other. The crystal structure of **1** by single-crystal X-ray analysis also supports this result in solution [3].

2.1.2. Synthesis of Complexes

In dnp, the coordination space of the equatorial position is narrower than that of the similar tpy. By using this steric feature, it is possible to impart selectivity when replacing the labile aqua ligand with another one. The aqua ligand of **1** was replaced with the rodlike molecule CH_3CN at room temperature to give the corresponding **2** (acetonitrile complex) (Figure 1a). In addition, **3** (benzonitrile (PhCN)-bound complex) formed in the reaction with PhCN, though PhCN contains a bulky phenyl group. It was confirmed by both X-ray structural and various spectroscopic analyses that the aqua ligand of **1** can be replaced by nitriles (see below). When a substitution reaction was performed using the linear thiocyanate anion (SCN^-) to investigate the effect of electronic repulsion between dnp and incoming ligands, corresponding **4** (SCN-coordinated complex) was obtained. Based on ^1H NMR and Electrospray ionization mass spectrometry (ESI-MS) analyses, the SCN ligand in **4** was observed to be coplanar with dnp. It is well-known that SCN^- is an ambidentate ligand. Although we could not

identify the coordination atom from the infrared spectrum data ($\nu_{N\equiv C}$ = 2134 cm^{-1}) of **4**, SCN^- would likely coordinate with its smaller (relative to sulfur) nitrogen atom in **4** because SCN^- was coordinated selectively to the ruthenium center at the nitrogen atom in a similar complex containing dnp [10].

On the other hand, the aqua ligand of **1** did not exchange with the nitrite ion (NO_2^-), which is another ambidentate ligand; instead, the axial ligand (PPh_3) underwent substitution to produce **5** (Figure 1b). Two characteristic bands in the fingerprint region (1438 and 1304 cm^{-1}) from the IR (infrared) spectrum of **5** suggest that **5** is a nitrogen atom-coordinated nitro species [11,12]. In addition to NO_2^-, **1** reacted with halide ions Cl^- and Br^- to give the axial ligand-substituted **6** (chlorido complex) and **7** (bromido complex), respectively. It was confirmed by both ^1H NMR and mass spectral analyses that complexes **5**–**7** each have one PPh_3 ligand and retain the aqua ligand.

Figure 1. Synthetic routes for complexes **2**–**8**. Eq-subst. and ax-subst. denote equatorial position substitution and axial position substitution, respectively.

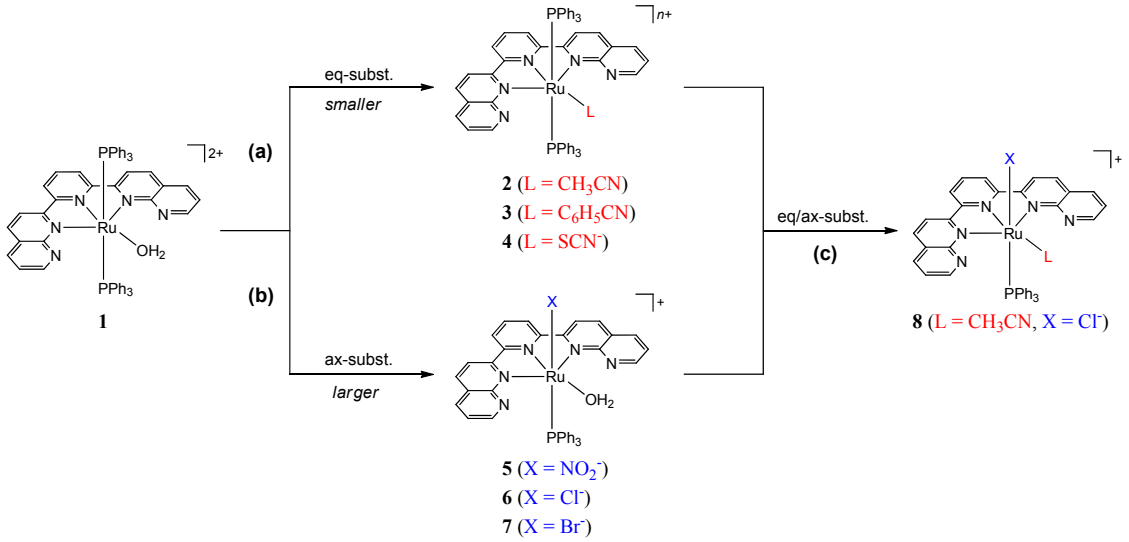

Reaction of the acetonitrile-substituted complex with chloride (*i.e.*, **2** and Cl^-) and the chlorido complex with acetonitrile (*i.e.*, **6** and CH_3CN) both lead to **8** (double-substituted complex) (Figure 1c). To summarize, the synthetic reactions using **1** are classified into two groups based on the combination of size selectivity of dnp and complementarity of size and shape of the incorporated molecule. The ligand having both linear molecular shape and smaller coordination atoms (the second period elements) incorporates into the coordination space of dnp to replace the coordinated water molecule (Figure 1a). On the other hand, nonlinear molecules or the third or later period elements are unable to approach the coordination space of dnp. As a result, an axial ligand, rather than the aqua ligand, is involved in the substitution reaction (Figure 1b). Thus, the supporting dnp acts as a so-called "molecular sieve."

2.2. Spectral and Structural Features of the Complexes

2.2.1. Electronic Absorption Spectra

The electronic absorption spectral data for the series complexes are summarized in Table 1. The complexes exhibit intense high-energy $d\rightarrow\pi^*$ metal-to-ligand charge transfer (MLCT) and $\pi\rightarrow\pi^*$ intraligand transitions in the UV region. The weak UV absorptions observed in the 310–360 nm range have been assigned to unresolved ligand-field $d\rightarrow d$ transitions on the ruthenium(II) center. In addition, the stronger visible transitions in the 370–600 nm range have been assigned to low-energy MLCT transitions [13]. Dnp may be considered as a dipyrido-fused analogue of tpy, which is both more delocalized and more electronegative [14]. As a result, dnp is a much better charge acceptor. This difference is evidenced by the absorption maxima of **8** and the corresponding terpyridine analogue ($[Ru(tpy)(PPh_3)(CH_3CN)Cl]^+$), where the latter (tpy-complex) MLCT band is at 466 nm [15], and **8** absorbs at 563 nm. It is worth noting that the more planar system gives rise to a better delocalization and consequently exhibits lower energy absorption.

Table 1. Electronic absorption data for complexes **1**–**8** [a].

Complex	λ_{max}/nm (ε/M^{-1} cm^{-1})			Solvent
1	523 (3500) 327 (22400)	373 (16700)	355 (15800)	acetone
2	477 (3100) 319 (24300)	374 (20400) 274 (42000)	356 (16300)	methanol
3	492 (4300) 312 (28700)	453 (4600)	372 (18600)	methanol
4	547 (3400) 279 (28800)	373 (12800)	321 (19100)	acetonitrile
5	551 (4100) 327 (18800)	370 (15900)	343 (18800)	acetone
6	580 (3700)	352 (19900)	330 (27400)	acetone
7	590 (4600)	350 (25500)	327 (21800)	acetone
8	563 (3400) 320 (25300)	374 (15800) 240 (37200)	353 (18600)	methanol

[a] $c = 1.0 \times 10^{-4}$ M.

Figure 2 shows the visible absorption spectra of $[Ru(dnp)(PPh_3)(OH_2)X]^{n+}$-type aqua complexes (X = PPh_3: **1**, NO_2: **5**, Cl: **6**, and Br: **7**) in acetone solution. The MLCT bands of anion-bound complexes (**5**, **6**, and **7**) are red-shifted with regard to the corresponding **1** (phosphine complex) because of the relative destabilization of $d\pi$(Ru) levels caused by the anionic ligands. The relative shifts in the MLCT transitions to lower energies ($X = Br^- < Cl^- < NO_2^- < PPh_3$) follow the spectrochemical series. Ligand variation has altered the MLCT band energies, suggesting that substitution of these ligands moves the $d\pi$ orbital energies of the ruthenium(II) metal center.

Figure 2. Visible absorption spectra of aqua complexes **1** and **5**–**7** (1.0×10^{-4} M in acetone).

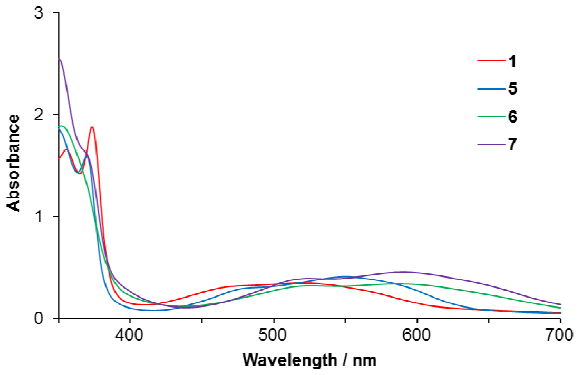

2.2.2. Molecular Structures

Single-crystal X-ray analyses of the nitrile complexes (**2**, **3**, and **8**) have been conducted to understand the geometry of series complexes in detail. The molecular structure of **1** has been reported elsewhere [3]. Selected parameters are summarized in Table 2, and the ORTEP diagrams for these cations are shown in Figures 3–5. All of the Ru–N distances of dnp are in the range 2.118(2)–2.167(6) Å with the exception of the central Ru–N bond, which is shorter (1.9660(14)–2.007(7) Å), as expected (Table 2). The phosphine ligands are in axial positions with respect to the tridentate dnp. The Ru–P bond distances of bis-phosphine complexes (2.4306(7) Å for **2**, 2.430(2) and 2.436(2) Å for **3**) are longer than that of the 2.3272(7) Å distance in **8**, which has a *trans* chlorido ligand. However, these distances are in the range previously observed in Ru(II)-phosphine complexes [15–18]. The nitrile units (N≡CR) are essentially linear and the Ru–N, N–C, and C–C bond distances are similar to typical values in other Ru(II)-N≡CR complexes [15]. The phenyl ring of benzonitrile in **3** is nearly coplanar with dnp; the dihedral angle between the central pyridyl ring and the phenyl ring is 13.0(4)°. This geometry is attributed to steric hindrance between the phenyl rings of PPh_3 and PhCN. In addition, the bond distance of Ru–Cl (2.4412(7) Å) in **8** is within the typical range for Ru(II)-chlorido complexes bearing tridentate pyridyl ligands [15].

Table 2. Selected bond distances (Å) and angles (°) for **2**, **3**, and **8**.

Parameter	**2**		**3**		**8·2H$_2$O**	
Bond distances	Ru1-P1	2.4306(7)	Ru1-P1	2.436(2)	Ru1-P1	2.3272(7)
	Ru1-N2	2.118(2)	Ru1-P2	2.430(2)	Ru1-Cl1	2.4412(7)
	Ru1-N3	1.968(2)	Ru1-N2	2.167(6)	Ru1-N2	2.1206(15)
	Ru1-N4	2.051(2)	Ru1-N3	2.007(7)	Ru1-N3	1.9660(14)
	N4-C30	1.123(4)	Ru1-N4	2.163(6)	Ru1-N4	2.1442(15)
	C30-C31	1.464(5)	Ru1-N6	2.042(8)	Ru1-N6	2.0517(15)
	-	-	N6-C22	1.141(12)	N6-C40	1.130(3)
	-	-	C22-C23	1.438(14)	C40-C41	1.465(3)
Bond angles	Ru1-N4-C30	180.0	Ru1-N6-C22	179.3(6)	Ru1-N6-C40	174.2(3)
	N4-C30-C31	180.0	N6-C22-C23	176.3(9)	N6-C40-C41	178.2(3)
Dihedral angle[a]	-	-	-	13.0(4)	-	-

[a] The central pyridyl ring of dnp *vs.* the phenyl ring of benzonitrile.

Figure 3. Molecular structure of the cation in complex **2**. Counteranions and hydrogen atoms are omitted for clarity.

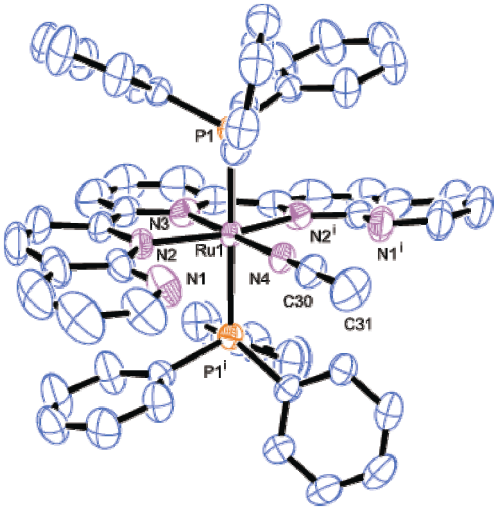

Figure 4. Molecular structure of the cation in complex **3**. Counteranions and hydrogen atoms are omitted for clarity.

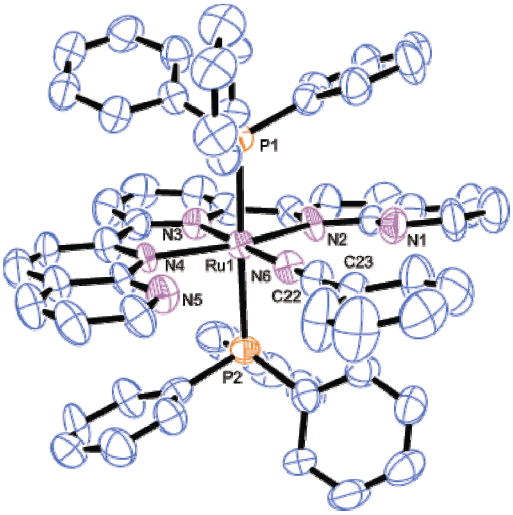

Figure 5. Molecular structure of the cation in complex **8**. The counteranion, solvent molecules, and hydrogen atoms are omitted for clarity.

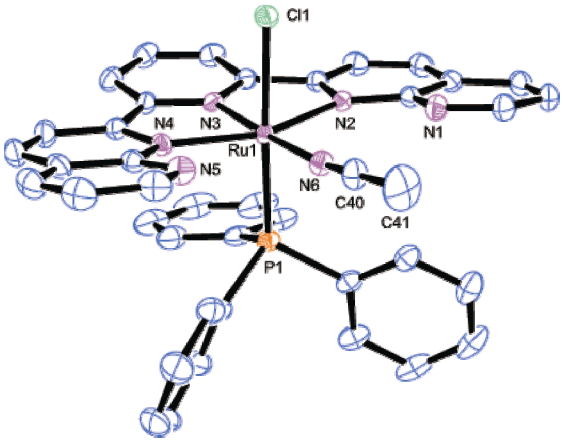

A remarkable structural feature is that the interatomic distances between noncoordinating nitrogen atoms of dnp are short. As described above, the complex system contains dnp that has two naphthyridine moieties on both sides of pyridine. The additional naphthyridine moieties could cause significant steric hindrance for Cl^- binding in **1** (or **2**). Thus, the presence of dnp seems to influence the selective coordination to the equatorial position. To examine this steric effect, density functional theory (DFT) calculations have been performed on **8** (and its geometrical isomer **8′**). The DFT-optimized structure for **8** is similar to its experimental structure. For example, for **8**, the calculated Ru–N and N–C bond distances and the angle of N–C–C in the acetonitrile ligand are 2.09 Å, 1.15 Å, and 179.5°, respectively, which are comparable to the experimental values (Table 2). Figure 6 depicts the optimized structures of **8** and **8′** and demonstrates greater steric hindrance at the equatorial ligand plane of **8′** than **8**. There is a large calculated energy difference between **8** and **8′**. **8** prefers *trans*-P, Cl geometry, which is 14.1 kcal/mol lower than that of **8′**. As shown in Figure 6, this geometrical preference is due to the narrower coordination space generated by the naphthyridine moieties in **8**, which prefers a linear CH_3CN coordination. This calculated result is strongly in accord with the fact that **8′** does not experimentally form.

Figure 6. Space-filling models of the lowest energy structures of geometrical isomers (**8** and **8′**) with the electronic energy difference.

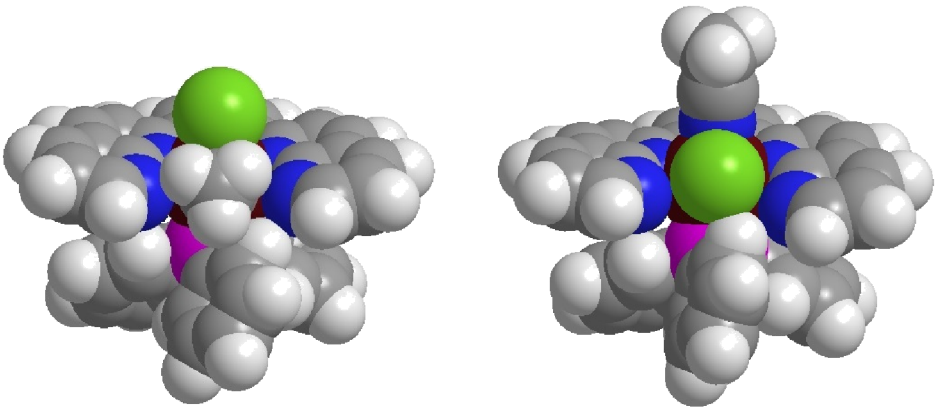

3. Experimental Section

3.1. Material and Methods

All solvents purchased for organic synthesis were anhydrous and used without further purification. Dnp [4,5] and $[RuCl_2(CH_3CN)_2(PPh_3)_2]$ [6] were prepared according to previously reported procedures.

Elemental analysis data were obtained on a Perkin Elmer 2400II series CHN analyzer. ^1H and $^{31}P\{^1H\}$ NMR spectra were recorded on a JEOL JMN-AL300 spectrometer (25 °C) operating at ^1H and ^{31}P frequencies of 300 and 121 MHz, respectively. ESI-MS data were obtained on a Bruker Daltonics microTOF. Electronic absorption spectra were obtained in 1-cm quartz cuvettes on a JASCO V-570 UV/VIS/NIR spectrophotometer. IR spectra were obtained using the KBr pellet method with a JASCO FT-IR 4100 spectrometer. DFT calculations were performed on **8** and **8′**. The ground-state,

gas-phase structures of these complexes were optimized at the DFT level (B3LYP) [19,20]. The DGDZVP basis set was used for Ru atoms [21,22]. The 6-31G(d) basis set was employed for H, C, N, P, and Cl atoms [23,24]. A vibrational analysis was carried out to confirm the optimized geometry is a true minimum with no imaginary frequency. All of the calculations were performed using the *Gaussian 09W* program package [25].

3.2. Synthesis of the Complexes

3.2.1. Synthesis of $[Ru(dnp)(PPh_3)_2(OH_2)](PF_6)_2$ (**1**)

An ethanolic solution (60 mL) containing $[RuCl_2(CH_3CN)_2(PPh_3)_2]$ (200 mg, 0.257 mmol), dnp (94 mg, 0.268 mmol), and PPh_3 (68 mg, 0.257 mmol) was refluxed for 2 h. The solution was filtered and evaporated to 10 mL under reduced pressure. An aqueous solution of KPF_6 was added and the mixture was allowed to cool overnight. The precipitate was collected by filtration, washed with diethyl ether, and dried *in vacuo*. The crude product was purified by column chromatography on Al_2O_3 (eluent: acetone). Yield: 148 mg (45%). Anal. Calcd. for $[Ru(dnp)(PPh_3)_2(OH_2)](PF_6)_2 \cdot CH_3CN$: $C_{59}H_{48}N_6OF_{12}P_4Ru$: C, 54.09; H, 3.69; N, 6.42. Found: C, 54.31; H, 3.79; N, 6.41%. ESI-MS (CH_3CN): *m/z* 349.5 ($[M–PPh_3–H_2O]^{2+}$), 358.5 ($[M–PPh_3]^{2+}$), 480.6 ($[M–H_2O]^{2+}$). ^{1}H NMR (acetone-d_6): δ 9.42 (dd, J = 4.5, 1.8 Hz, 2H, dnp), 8.69–8.59 (m, 6H, dnp), 8.43 (d, J = 8.7 Hz, 2H, dnp), 8.23–8.14 (m, 2H, dnp and H_2O), 8.02 (dd, J = 8.4, 4.2 Hz, 2H, dnp), 7.19 (t, J = 7.5 Hz, 6H, PPh_3), 6.91 (t, J = 9.0 Hz, 12H, PPh_3), and 6.79–6.73 (m, 12H, PPh_3) ppm. $^{31}P\{^1H\}$ NMR (acetone-d_6): δ 27.29 ppm.

3.2.2. Synthesis of $[Ru(dnp)(PPh_3)_2(RCN)](PF_6)_2$ (R = CH_3 (**2**); R = C_6H_5 (**3**))

An acetonitrile solution (30 mL) containing **1** (56 mg, 0.044 mmol) was stirred for 24 h at room temperature. The volume was reduced to 5 mL using a rotary evaporator, and orange crystals were precipitated by adding diethyl ether (20 mL). The precipitate was collected by filtration, washed with diethyl ether, and dried *in vacuo*. The crude product was finally recrystallized from acetonitrile and diethyl ether, yielding **2** as an orange powder. Yield: 49 mg (86%). Anal. Calcd. for $[Ru(dnp)(PPh_3)_2(CH_3CN)](PF_6)_2 \cdot H_2O$: $C_{59}H_{48}N_6OF_{12}P_4Ru$: C, 54.09; H, 3.69; N, 6.42. Found: C, 53.77; H, 3.68; N, 6.57%. ESI-MS (CH_3CN): *m/z* 349.6 ($[M–PPh_3–CH_3CN]^{2+}$), 480.6 ($[M–CH_3CN]^{2+}$). ^{1}H NMR (acetonitrile-d_3): δ 9.35 (dd, J = 4.5, 1.8 Hz, 2H, dnp), 8.31–8.26 (m, 4H, dnp), 8.20–8.17 (m, 2H, dnp), 8.07 (t, J = 8.1 Hz, 1H, dnp), 7.89–7.81 (m, 4H, dnp), 7.13 (t, J = 7.6 Hz, 6H, PPh_3), and 6.85–6.70 (m, 24H, PPh_3) ppm [26]. $^{31}P\{^1H\}$ NMR (acetonitrile-d_3): δ 31.16 ppm.

A similar reaction between **1** (50 mg, 0.039 mmol) and benzonitrile gave **3** with an 82% (52 mg) yield. Anal. Calcd. for $[Ru(dnp)(PPh_3)_2(C_6H_5CN)](PF_6)_2$: $C_{64}H_{48}N_6F_{12}P_4Ru$: C, 56.77; H, 3.57; N, 6.21. Found: C, 56.88; H, 3.41; N, 6.26%. ESI-MS (CH_3CN): *m/z* 349.6 ($[M–PPh_3–C_6H_5CN]^{2+}$), 480.6 ($[M–C_6H_5CN]^{2+}$). ^{1}H NMR (acetone-d_6): δ 9.47 (dd, J = 3.9, 1.8 Hz, 2H, dnp), 8.69–8.53 (m, 6H, dnp), 8.33 (d, J = 8.7 Hz, 2H, dnp), 7.94 (dd, J = 8.1, 3.9 Hz, 2H, dnp), 7.81 (t, J = 7.5 Hz, 1H, dnp), 7.21–7.16 (m, 7H, PPh_3 and PhCN), 6.96–6.89 (m, 26H, PPh_3 and PhCN), and 6.77–6.75 (m, 2H, PhCN) ppm. $^{31}P\{^1H\}$ NMR (acetone-d_6): δ 30.02 ppm.

3.2.3. Synthesis of [Ru(dnp)(PPh_3)$_2$(SCN)](PF_6) (**4**) and [Ru(dnp)(PPh_3)(OH_2)X](PF_6) (X = NO_2 (**5**), Cl (**6**), Br (**7**))

In a typical preparation, a methanolic solution (40 mL) containing **1** (50 mg, 0.039 mmol) and 1.1 equiv. of NaSCN (10 mg) was refluxed for 30 min. The volume was reduced to 5 mL and a saturated solution of KPF_6 was added. The resulting solid was filtered and then washed with water followed by diethyl ether. The crude product was recrystallized from acetone/diethyl ether. The yield was 32 mg (69%) for **4**. ESI-MS (CH_3CN): *m*/*z* 757.0 ([M–PPh_3]$^+$), 1019.1 ([M]$^+$). ^{1}H NMR (acetone-d_6): δ 9.54 (dd, *J* = 3.9, 1.8 Hz, 2H, dnp), 8.42–8.33 (m, 6H, dnp), 8.15 (d, *J* = 8.7 Hz, 2H, dnp), 8.03 (t, *J* = 8.1 Hz, 1H, dnp), 7.86 (dd, *J* = 8.1, 3.9 Hz, 2H, dnp), 7.14–6.99 (m, 18H, PPh_3), and 6.83 (t, *J* = 6.9 Hz, 12H, PPh_3) ppm. ^{31}P{^{1}H} NMR (acetone-d_6): δ 27.38 ppm. IR (KBr): 2134 cm^{-1} (*ν*N≡C).

A similar reaction between **1** and $NaNO_2$ under the same conditions described above gave **5** in 74% yield (26 mg). ESI-MS (CH_3CN): *m*/*z* 745.5 ([M–H_2O]$^+$). ^{1}H NMR (acetone-d_6): δ 9.50 (dd, *J* = 4.5, 1.8 Hz, 2H, dnp), 8.79–8.54 (m, 9H, dnp and H_2O), 8.13 (t, *J* = 8.1 Hz, 1H, dnp), 8.03 (dd, *J* = 4.8, 2.1 Hz, 2H, dnp), 7.20–7.16 (m, 3H, PPh_3), and 6.95–6.92 (m, 12H, PPh_3) ppm. ^{31}P{^{1}H} NMR (acetone-d_6): δ 38.33 ppm. IR (KBr): 1438, 1304 cm^{-1} (*ν*NO_2).

A similar reaction between **1** and Et_4NCl under the same conditions described above gave **6** in 67% yield (23 mg). ESI-MS (CH_3CN): *m*/*z* 734.1 ([M–H_2O]$^+$). ^{1}H NMR (acetone-d_6): δ 9.46 (dd, *J* = 4.5, 1.8 Hz, 2H, dnp), 8.74–8.70 (m, 4H, dnp), 8.57 (dd, *J* = 8.4, 1.8 Hz, 4H, dnp), 8.48 (s, 1H, H_2O), 8.05–7.91 (m, 3H, dnp), 7.20–7.13 (m, 3H, PPh_3), and 6.95–6.91 (m, 12H, PPh_3) ppm. ^{31}P{^{1}H} NMR (acetone-d_6): δ 43.11 ppm.

A similar reaction between **1** and Bu_4NBr under the same conditions described above gave **7** in 94% yield (35 mg). ESI-MS (CH_3CN): *m*/*z* 780.1 ([M–H_2O]$^+$), 808.1 ([M–H_2O+N_2]$^+$). ^{1}H NMR (acetone-d_6): δ 9.46 (dd, *J* = 4.5, 2.1 Hz, 2H, dnp), 8.74–8.70 (m, 4H, dnp), 8.59 (dd, *J* = 8.7, 2.1 Hz, 4H, dnp), 8.38 (s, 1H, H_2O), 8.06–7.98 (m, 3H, dnp), 7.20–7.16 (m, 3H, PPh_3), and 6.95–6.91 (m, 12H, PPh_3) ppm. ^{31}P{^{1}H} NMR (acetone-d_6): δ 43.32 ppm.

3.2.4. Synthesis of [Ru(dnp)(PPh_3)(CH_3CN)Cl]Cl (**8**)

An acetonitrile solution (30 mL) containing **1** (30 mg, 0.023 mmol) and Et_4NCl (8 mg, 0.048 mmol) was refluxed for 6 h. The volume was reduced to 5 mL using a rotary evaporator, and purple crystals were precipitated by adding diethyl ether (15 mL). The precipitate was collected by filtration, washed with diethyl ether, and dried *in vacuo*. The crude product was recrystallized from methanol/diethyl ether, yielding **8** as a violet powder. Yield: 15 mg (83%). Anal. Calcd. for [Ru(dnp)(PPh_3)(CH_3CN)Cl]Cl·3H_2O: $C_{42}H_{37}N_6O_3PRu$: C, 56.95; H, 4.31; N, 9.72. Found: C, 56.58; H, 4.23; N, 9.57%. ESI-MS (CH_3CN): *m*/*z* 734.1 ([M–CH_3CN]$^+$). ^{1}H NMR (acetonitrile-d_3): δ 9.34 (dd, *J* = 4.5, 1.8 Hz, 2H, dnp), 8.41–8.34 (m, 6H, dnp), 8.17 (d, *J* = 8.7 Hz, 2H, dnp), 8.03 (t, *J* = 8.1 Hz, 1H, dnp), 7.78 (dd, *J* = 8.1, 4.2 Hz, 2H, dnp), 7.15–7.08 (m, 3H, PPh_3), and 6.93–6.85 (m, 12H, PPh_3) ppm [26]. ^{31}P{^{1}H} NMR (acetonitrile-d_3): δ 46.95 ppm.

3.3. X-ray Crystallographic Analyses

Single crystals of the perchlorate salt of **2** and **8**·2H_2O were obtained by diffusion of diethyl ether into an acetonitrile solution of each of the complexes. Single crystals of **3** were obtained by diffusion of diethyl ether into a benzonitrile solution of the complex. An orange crystal of **2** with dimensions 0.30 × 0.30 × 0.15 mm, an orange crystal of **3** with dimensions 0.20 × 0.10 × 0.05 mm, and a deep violet crystal of **8**·2H_2O with dimensions 0.30 × 0.25 × 0.25 mm were mounted on a glass fiber. Measurements were made on a Rigaku RAXIS-RAPID diffractometer with graphite monochromated Mo Kα radiation (λ = 0.71075 Å). Data were collected to a maximum 2θ value of 55°. All calculations were conducted using the *CrystalStructure* crystallographic software package [27] except for refinement, which was performed using *SHELXL97* [28]. The structures were solved by direct methods [29,30] and were expanded using Fourier techniques. Multi-scan absorption corrections were applied [31]. The non-hydrogen atoms were refined anisotropically, and hydrogen atoms were included as raiding atoms. Crystallographic parameters of **2**, **3**, and **8**·2H_2O are summarized in Table 3. Crystallographic data have been deposited with the Cambridge Crystallographic Data Centre as Supplementary Publication Nos. CCDC-962347 for **2**, 962348 for **3**, and 962349 for **8**·2H_2O.

Table 3. Crystallographic data for **2**, **3**, and **8**·2H_2O.

Parameter	**2**	**3**	**8·2H_2O**
Chemical formula	$C_{59}H_{46}N_6O_8Cl_2P_2Ru$	$C_{64}H_{48}N_6F_{12}P_4Ru$	$C_{41}H_{35}N_6O_2Cl_2PRu$
Formula weight	1200.97	1354.07	846.72
Temperature (K)	296(1)	296(1)	173(1)
Crystal system	monoclinic	monoclinic	Monoclinic
Space group	*C*2/*c*	*Cc*	*C*2/*c*
Unit cell parameters			
a (Å)	17.7754(3)	17.1743(4)	26.4297(5)
b (Å)	13.2405(2)	16.1763(4)	16.2228(3)
c (Å)	22.6972(4)	21.0790(4)	19.4965(4)
B (°)	96.4561(7)	97.8336(7)	114.9980(7)
V (Å^3)	5308.03(15)	5801.5(2)	7576.3(3)
Z	4	4	8
Calculated density (g cm^{-3})	1.503	1.550	1.485
μ (Mo Kα) (mm^{-1})	0.520	0.468	0.642
No. of measured reflections	25463	46099	34745
No. of observed reflections	6075	12645	8632
Refinement method	*Full-matrix least-squares on F^2*		
Parameters	356	785	474
*R*1 ($I > 2\sigma(I)$) [a]	0.0444	0.0580	0.0311
w*R*2 (all data) [b]	0.1292	0.2164	0.0803
S	1.050	1.126	1.038

[a] $R1 = \sum||F_o| - |F_c||/\sum |F_o|$; [b] $wR2 = \{\sum_w(F_o^2 - F_c^2)^2/\sum_w(F_o^2)^2\}^{1/2}$.

4. Conclusions

We have described the synthesis and X-ray crystallographic characterization of a new ruthenium complex system containing the highly functional dnp ligand. Computational analysis suggests that the incorporation of dnp not only stabilizes the complex but also enables this system to be synthesized with improved stereospecificity. The results provide useful information to elucidate this facile and selective synthetic approach to new transition metal complexes. For example, regulation of linkage isomerization in ruthenium complexes involving SCN^- could contribute to materials science in the development of photosensitizers for dye-sensitized solar cells (DSCs).

Acknowledgments

We thank the Foundation for Japanese Chemical Research (424-R) for financial support. Moreover, we are grateful to R. Naoi of Fukushima University for assistance with the spectroscopic measurements.

Conflicts of Interest

The authors declare no conflict of interest.

References

1. Chowdhury, A.D.; Das, A.; Irshad, K.; Mobin, S.M.; Lahiri, G.K. Isomeric complexes of $[Ru^{II}(trpy)(L)Cl]$ (trpy = 2,2':6',2"-terpyridine and HL = quinaldic acid): Preference of isomeric structural form in catalytic chemoselective epoxidation process. *Inorg. Chem*. **2011**, *50*, 1775–1785.
2. Dakkach, M.; López, M.I.; Romero, I.; Rodríguez, M.; Atlamsani, A.; Parella, T.; Fontrodona, X.; Llobet, A. New Ru(II) complexes with anionic and neutral N-donor ligands as epoxidation catalysts: An evaluation of geometrical and electronic effects. *Inorg. Chem*. **2010**, *49*, 7072–7079.
3. Oyama, D.; Yamanaka, T.; Fukuda, A.; Takase, T. Modulation of intramolecular hydrogen bonding strength by axial ligands in ruthenium(II) complexes. *Chem. Lett.* **2013**, *42*, 1554–1555.
4. Campos-Fernández, C.S.; Thomson, L.M.; Galán-Mascarós, J.R.; Ouyang, X.; Dunbar, K.R. Homologous series of redox-active, dinuclear cations $[M_2(O_2CCH_3)_2(pynp)_2]^{2+}$ (M = Mo, Ru, Rh) with the bridging ligand 2-(2-pyridyl)-1,8-naphthyridine (pynp). *Inorg. Chem.* **2002**, *41*, 1523–1533.
5. Tseng, H.-W.; Zong, R.; Muckerman, J.T.; Thummel, R. Mononuclear ruthenium(II) complexes that catalyze water oxidation. *Inorg. Chem.* **2008**, *47*, 11763–11773.
6. Al-Far, A.M.; Slaughter, L.M. *cis-cis-trans*-Bis(acetonitrile-κ*N*)dichloridobis(triphenylphosphine-κ*P*)ruthenium(II) acetonitrile disolvate. *Acta Crystallogr.* **2008**, *E64*, m184.
7. Kaveevivitchai, N.; Zong, R.; Tseng, H.-W.; Chitta, R.; Thummel, R.P. Further observations on water oxidation catalyzed by mononuclear Ru(II) complexes. *Inorg. Chem.* **2012**, *51*, 2930–2939.
8. Suen, H.F.; Wilson, S.W.; Pomerantz, M.; Walsh, J.L. Photosubstitution reactions of terpyridine complexes of ruthenium(II). *Inorg. Chem.* **1989**, *28*, 786–791.
9. Zong, R.; Naud, F.; Segal, C.; Burke, J.; Wu, F.; Thummel, R. Design and study of bi[1,8]naphthyridine ligands as potential photooxidation mediators in Ru(II) polypyridyl aquo complexes. *Inorg. Chem*. **2004**, *43*, 6195–6202.

10. Oyama, D.; Yamanaka, Y.; Watanabe, Y.; Takase, T. Fukushima University, Fukushima, Japan. Unpublished work, 2013.
11. Nakamoto, K. *Infrared and Raman Spectra of Inorganic and Coordination Compounds*, 4th ed.; John Wiley & Sons: New York, NY, USA, 1986; pp. 221–227.
12. Ooyama, D.; Nagao, N.; Nagao, H.; Miura, Y.; Hasegawa, A.; Ando, K.-I.; Howell, F.S.; Mukaida, M.; Tanaka, K. Redox- and thermally-induced nitro-nitrito linkage isomerizations of ruthenium(II) complexes having nitrosyl as a spectator ligand. *Inorg. Chem.* **1995**, *34*, 6024–6033.
13. Juris, A.; Balzani, V.; Barigelletti, F.; Campagna, S.; Belser, P.; von Zelewsky, A. Ru(II) polypyridine complexes: Photophysics, photochemistry, electrochemistry, and chemiluminescence. *Coord. Chem. Rev*. **1988**, *84*, 85–277.
14. Thummel, R.P.; Decloitre, Y. Polyaza cavity-shaped molecules. VIII. Ruthenium(II) complexes with 3,3'-annelated derivatives of 2-(2'-pyridyl)quinoline and 2-(2'-pyridyl)-1,8-naphthyridine. *Inorg. Chim. Acta* **1987**, *128*, 245–249.
15. Ooyama, D.; Saito, M. Synthesis, characterization and reactivity of polypyridyl ruthenium(II) carbonyl complexes with phosphine derivatives: ruthenium-carbon bond labilization based on steric and electronic effects. *Inorg. Chim. Acta* **2006**, *359*, 800–806.
16. Chen, J.; Szalda, D.J.; Fujita, E.; Creutz, C. Iron(II) and ruthenium(II) complexes containing P, N, and H ligands: structure, spectroscopy, electrochemistry, and reactivity. *Inorg. Chem.* **2010**, *49*, 9380–9391.
17. Ooyama, D.; Sato, M. A synthetic precursor for hetero-binuclear metal complexes, $[Ru(bpy)(dppy)_2(CO)_2](PF_6)_2$ (bpy = 2,2'-bipyridine, dppy = 2-(diphenylphosphino)pyridine). *Appl. Organomet. Chem.* **2004**, *18*, 380–381.
18. Ooyama, D.; Sato, M. Crystal structure of (2,2'-bipyridine-*N,N'*)(diphenyl-2-phosphinopyridine-*P*)chloro(dicarbonyl)ruthenium(II) hexafluorophosphate. *Anal. Sci.* **2003**, *19*, x39–x40.
19. Becke, A.D. Density-functional thermochemistry. III. The role of exact exchange. *J. Chem. Phys.* **1993**, *98*, 5648–5652.
20. Lee, C.; Yang, W.; Parr, R.G. Development of the Colle-Salvetti correlation-energy formula into a functional of the electron density. *Phys. Rev. B* **1988**, *37*, 785–789.
21. Sosa, C.; Andzelm, J.; Elkin, B.C.; Wimmer, E.; Dobbs, K.D.; Dixon, D.A. A local density functional study of the structure and vibrational frequencies of molecular transition-metal compounds. *J. Phys. Chem.* **1992**, *96*, 6630–6636.
22. Godbout, N.; Salahub, D.R.; Andzelm, J.; Wimmer, E. Optimization of Gaussian-type basis sets for local spin density functional calculations. Part I. Boron through neon, optimization technique and validation. *Can. J. Chem*. **1992**, *70*, 560–571.
23. Hehre, W.J.; Ditchfield, R.; Pople, J.A. Self-consistent molecular orbital methods. XII. Further extensions of Gaussian-type basis sets for use in molecular orbital studies of organic molecules. *J. Chem. Phys.* **1972**, *56*, 2257–2261.
24. Francl, M.M.; Pietro, W.J.; Hehre, W.J.; Binkley, J.S.; Gordon, M.S.; DeFrees, D.J.; Pople, J.A. Self-consistent molecular orbital methods. XXIII. A polarization-type basis set for second-row elements. *J. Chem. Phys.* **1982**, *77*, 3654–3665.

25. Frisch, M.J.; Trucks, G.W.; Schlegel, H.B.; Scuseria, G.E.; Robb, M.A.; Cheeseman, J.R.; Scalmani, G.; Barone, V.; Mennucci, B.; Petersson, G.A.; *et al. Gaussian 09W*, revision D.01; Gaussian, Inc.: Wallingford, CT, USA, 2009.
26. Methyl protons of both complexes could not be assigned due to their overlapping with solvent signals.
27. Rigaku. *CrystalStructure*, Version 3.8; Rigaku and Rigaku Americas: Woodlands, TX, USA, 2007.
28. Sheldrick, G.M. *SHELX*, SHELXL-97; University of Göttingen: Göttingen, Germany, 1997.
29. Altomare, A.; Cascarano, G.; Giacovazzo, C.; Guagliardi, A.; Burla, M.; Polidori, G.; Camalli, M. *SIR92*—A program for automatic solution of crystal structures by direct methods. *J. Appl. Crystallogr.* **1994**, *27*, 435.
30. Altomare, A.; Burla, M.; Camalli, M.; Cascarano, G.; Giacovazzo, C.; Guagliardi, A.; Molitern, A.; Polidori, G.; Spagna, R. *SIR97*: A new tool for crystal structure determination and refinement. *J. Appl. Crystallogr.* **1999**, *32*, 115–119.
31. Higashi, T. *ABSCOR*; Rigaku Corporation: Tokyo, Japan, 1995.